Effect of Intracrystalline Silanol Defects on the Diffusivity of Benzene in Silicalite Zeolite

Alechania Misturini, Omer F. Altundal, Pablo García-Aznar, Sara Kariminasab, and German Sastre*

Supporting Information available online

Dedicated to Prof. Dr. rer. nat. Jörg Kärger on the occasion of his 80th birthday

Intracrystalline zeolite silanol defect groups ($\equiv$SiOH) were modelled in silicalite (silica ZSM-5, MFI) using experimental data. We make a molecular dynamics study on the self-diffusivity of benzene in silicalite with defects. The simulations at three different loadings (1, 3 and 5 benzene per unit cell) and temperatures (298, 348 and 398 K) allow to calculate self-diffusivity, adsorption energy and the activation energy. The results show that benzene self-diffusivity in silicalite is increased by the presence of silanol defects. Previous experimental results support this claim.

Keywords: Benzene, Diffusion, Molecular dynamics, Silicalite, Zeolite defects

1 Introduction

Zeolites are a family of microporous solids, which are commonly utilized in industrial applications such as ion-exchange, heterogeneous catalysis, gas adsorption and separation due to their diverse structural characteristics, such as various pore sizes and shapes, chemical compositions and topologies [1, 2]. The structure of zeolites consists of corner sharing $TO_{4/2}$ tetrahedra as the main building unit, in which T is commonly either Si or Al.

In the synthesis of zeolites, organic structure directing agents (OSDAs) are usually employed to promote the formation of a specific zeolite phase. Since OSDAs are usually positively charged molecules, the net charge needs to be balanced in the zeolite framework. In aluminosilicate zeolites, charge is generally counterbalanced through the negative charge of the $[AlO_{4/2}]^-$ tetrahedra, whereas in pure silica structures, consisting of SiO_2 units, the neutrality is achieved by structural defects, such as those containing intracrystalline silanols ($\equiv$SiOH) and siloxy ($\equiv$SiO$^-$) groups [3].

Upon calcination of the OSDA molecules, the number of defects in zeolite structures has been demonstrated to reduce considerably, except for those with intrinsic silanol groups such as SSZ-74 [4], which includes ordered vacancy defects in its framework that do not heal upon calcination. For example, the high concentration of defects in ITQ-1 (33 % of the silicons belonged to defect sites) was reduced

to 6.9 % after the calcination [5]. In a similar work, these defects were seen to completely heal after calcination, resulting in a defect-free pure silica MWW structure [6]. The healing of defects after calcination was also observed in other zeolites such as MFI [7, 8], RTH [9], FER [10], SOD [11] and FAU [12].

The characterization of the defects in a zeolite can be done by ^{29}Si magic angle spinning (MAS) NMR through the information about Q^4 and Q^3 peaks, corresponding to a fully framework-coordinated silicon and to silicons with a network termination, respectively. If this termination is a OH group, this becomes an intracrystalline silanol defect, which will be considered in this study and can also be detected by ^{1}H MAS NMR. Further, cross polarization ^{29}Si/^{1}H allows a full identification of silanols [13]. By using this technique, Koller et al. [14] elucidated the chemistry of defects in DDR, MTW, AFI and MFI structures and

[1]Dr. Alechania Misturini
https://orcid.org/0000-0002-5873-8679,
[1]Omer F. Altundal https://orcid.org/0000-0002-2305-6088,
[1]Pablo García-Aznar https://orcid.org/0000-0003-0586-0037,
[1]Sara Kariminasab,
[1]Dr. German Sastre https://orcid.org/0000-0003-0496-6331
(gsastre@itq.upv.es)
[1]Instituto de Tecnología Química, Universitat Politècnica de València, Avda. de los Naranjos s/n, 46022 Valencia, Spain.

concluded that the optimum place for defects in these structures are the six rings and proposed a model for the defect sites. Later, by analyzing double quantum and triple quantum ^{1}H MAS NMR of as-made ZSM-5, Brunklaus et al. [15] determined the arrangement of the defects in MFI structure and suggested that defects should be located in edge-sharing 6-rings along the straight channels.

Silanols have been used for various applications. For example, silanol groups can be formed by hydrolysis of certain germanosilicates, such as UTL, playing an important role in synthesis of novel zeolite phases using assembly-disassembly-organization-reassembly (ADOR) process [16]. Moreover, the presence of silanol defects may alter the structural and chemical properties of zeolites, thus they have been a topic of interest for material scientists [17]. While studying the catalytic activity of silicalite, Janiszewska et al. [18] discovered that silanol nests increase the conversion of propan-2-ol to propylene. After exploring the methanol-to-olefin (MTO) process over Sigma-1 and ZSM-58 zeolites (both structures with DDR topology), Yarulina et al. [19] concluded that internal silanols increase the deactivation rate of the MTO process. A similar result was obtained by Qin and co-workers, where the existence of silanol defects was responsible for the fast deactivation of the catalyst during methanol to hydrocarbon transformation [20]. Li et al. [21] used silanol-rich IPC-1P zeolite as support for rhodium nanoparticles and found out that silanol nests stabilize Rh particles due to hydrogen transfer between rhodium particles and silanols. As evidenced from these studies along with many others [22–26], the role of silanol groups on the catalytic performance of zeolites have been widely explored. However, their influence on the diffusive properties of zeolites is yet to be fully unveiled.

Self-diffusion of aromatics in zeolites has been widely explored experimentally, using methods such as quasielastic neutron scattering (QENS) and pulse field gradient nuclear magnetic resonance (PFG NMR) [27–30]. While these methods are the most accurate techniques for measuring self-diffusion, they are time-consuming and expensive. Computational methods like Monte Carlo (MC) and molecular dynamics (MD) simulations have proven to be very effective for calculating the self-diffusivity of molecules inside a zeolite in a time-efficient manner [31–33].

Motivated by this, in the present work we aim to reveal the effect of intracrystalline silanol defects on the self-diffusivity of benzene inside silicalite zeolite, a commercially available and industrially relevant material [34, 35], by computational methods. We introduced structural defects to the experimentally reported structure of as made ZSM-5 [36] according to the insights gained from refs. [14] and [15] and generated a defective silicalite structure (Fig. 1). We performed MD simulations using both defectless and defective silicalite zeolites at various temperatures and benzene loadings to investigate the effect of defects on the diffusion of benzene inside the silicalite zeolite.

The choice of system was also made so that high quality experimental data on self-diffusivity is available in the literature. QENS and PFG NMR [37] are able to investigate diffusion events typically in the interval of 2–35 ms [38]. QENS is considered as a microscopic procedure and information about diffusion mechanism at the atomic level can be obtained by this method. PFG NMR is also categorized as a microscopic technique and was introduced in the seventies, among others, by the Kärger group in Leipzig [39]. Jörg Kärger and Jürgen Caro presented a seminal paper which raised a decades-long debate about the large span of diffusivity values and types of diffusivities measured by the different techniques [40]. The study of complex systems can provide good insights into the mobility and transport phenomena of adsorbed molecules by application of these techniques [41]. Depending on the conditions of measurement provided by the host-guest system under study, the covered distances range from hundreds of nanometers to hundreds of micrometers. Thus, PFG NMR has the unique ability to determine the rate of molecular transport as a function of the distance traveled. With root-mean square displacements much smaller than the diameters of the crystals, the resulting diffusivities may unambiguously be attributed to the intracrystalline pore space. In addition, with increasing observation times and, correspondingly, increasing displacements, it becomes possible to obtain information about transport resistances at the external crystal surface and about long-range diffusivities, i.e., about the rate of transport through a bed of crystals/particles [30]. The measurements by PFG NMR as well as QENS, and also NSE (neutron spin echo) are done upon equilibrium conditions so that the self-diffusivity or tracer diffusivity can be obtained accordingly, although differences between the results by PFG NMR and QENS can be expected, if the spacings of the internal transport barriers lie between the distances of the mean diffusion path covered by QENS (typically a few nanometers) and PFG NMR (typically from hundreds of nanometers up to hundreds of micrometers) [42].

2 Computational Methods and Models

2.1 Models of Silicalite

The structure of pure silica ZSM-5, without defects, which will be called 'defectless', was taken from the work of Olson et al. [36]. To generate a model for the defective silicalite, silanol groups were introduced to the defectless ZSM-5 structure by considering the geometry and position of the defect sites proposed by Koller et al. [14] and Brunklaus et al. [15]. They reported that in this structure, containing a large number of 5-rings and without 4-rings, the silanol defects are stabilized in 6-rings. In particular, the 6-rings of ZSM-5 form aggregates of four edge-sharing 6-rings (Fig. 1a), in which defects are located during the synthesis process. Since a negative charge in the defect has to be

present in order to compensate each of the tetra-propyl-ammonium cations used as organic structure directing agent, it was suggested that a siloxy group ($\equiv$SiO$^-$) would be present per defect site, such as the one shown in Fig. 1b. Cross polarization ^{1}H ^{29}Si MAS NMR experiments allowed to establish that three silanol groups per siloxy were present and hence the defect structure indicated in Fig. 1b was suggested for the as-made silicalite. Upon calcination, as indicated in the introduction, most of the silanol defects are healed and ^{29}Si MAS NMR allows to establish four silanols per unit cell (u.c.). The corresponding defect is shown in Fig. 1c, and the above abundance corresponds to two defect sites, each containing two silanols, per u.c. (Fig. S2, Supporting Information). This is the model of silicalite with defects that will be used for the molecular dynamics simulations. A corresponding CIF file and further information is included in the Supporting Information (SI).
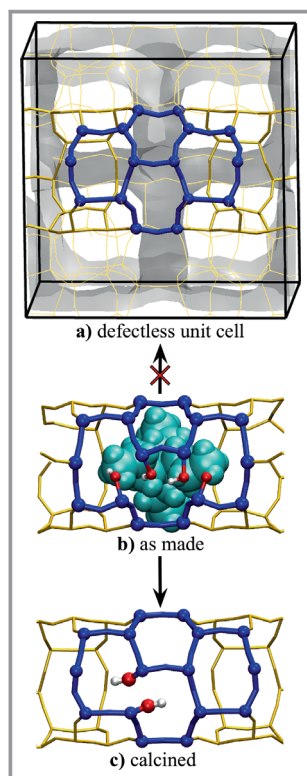
Figure 1. a) and c) Models of silicalite considered in this study. Starting from the (b) as-made material containing four clusters of defects – one of them shown in the image –, one per each OSDA (in cyan) molecule, calcination may produce either a) a defectless zeolite or c) a zeolite with defects. In the case of silicalite, unless the synthesis is made in fluoride media, calcination leads to a structure with 4 silanols per u.c., which are located in four edge-sharing 6-rings (colored in blue) according to cross polarization ^{1}H ^{29}Si MAS NMR data from by Koller et al. [14] and Brunklaus et al. [15].

2.2 Quantum Chemistry Calculations

A cluster model related to the defect in as-made silicalite (Fig. 1b) was generated. This cluster changed the siloxy group to a silanol since the protonation happens during the calcination, followed by a condensation reaction between two neighboring silanols.

This condensation reaction was modeled by means of Gaussian 16 package [43], using quantum chemistry semi-empirical PM7 method [44] in order to elucidate the activation barrier and the mechanism for this important process. The cluster was modeled by fixing the position of the outermost atoms (to mimic the inclusion in the crystal structure) and then minimized in energy.

The quantum semi-empirical PM7 [44] method includes dispersion parameters based on the parameters by Jurecka et al. [45], as well as previous dispersion corrections PM6-DH [46], PM6-DH2 [47] and PM6-D3H4 [48], for PM6 method, as a post-SCF correction. This method has been parametrized with Hobza's benchmark database S22 set [49], which provides extensive reference data for intermolecular interactions. While the previous post-SCF corrections accurately predict intermolecular interaction energy in those PM6-D methods, they fail considerably in predicting heats of formation. In PM7, the dispersion and hydrogen bond corrections were incorporated into the method before any parameter optimization was performed, so it is designed to reproduce both intermolecular interaction energies and heats of formation with accuracy. The parametrization of intermolecular interactions in this method has been proven to be more accurate, with lower average unsigned errors, than the predecessor PM6.

The transition state (TS) structure was elucidated with a frequency calculation, obtaining a single imaginary vibrational eigenvalue, whose atom contributions correspond to the reaction pathway. This was furthermore confirmed via an intrinsic reaction coordinate analysis [50], which led to the associated minima corresponding to both reactants and products, supporting the proposed TS as a saddle point between them.

2.3 Molecular Dynamics Simulations

The investigation of the benzene diffusion inside ZSM-5 structures was carried out by MD simulations, using DL_POLY Classic 2.20 software [51]. In order to make an appropriate description of the system, 2×2×2 unit cells were generated for both defectless and defective ZSM-5. The Verlet-leapfrog integration algorithm was utilized in all MD simulations, which were performed in the NVT ensemble [52]. The Nosé-Hoover thermostat was considered in the NVT-MD simulations to control the temperature [53]. In the simulations, both a flexible and a rigid zeolite model are used to explain the natural breathing and the thermal vibrations of zeolite channels, and to represent the experimentally measured pore diameter, respectively [54]. A timestep of 1 fs was employed in the simulations, where an equilibration of 20 ps was followed by a production run of 50 ns and 100 ns for rigid and flexible simulations, respectively. The

electrostatic interactions were modeled by the Coulomb potential [55], and Ewald summation was used for the calculation of long-range Coulombic interactions [56]. A cutoff of 9.0 Å was set for the truncation of nonbonded interactions, which were defined by the Lennard-Jones potential [57]. The intramolecular parameters for benzene molecules were taken from the fully flexible force field of Oie et al. [58], and point charges of $0.148\,e^-$ and $-0.148\,e^-$ were considered for H and C atoms, respectively. The optimized potentials for liquid simulations (OPLS) [59] all-atom force field, which has been parameterized for liquid benzene, was used to model nonbonded benzene···benzene interactions. The description of zeolite···benzene interactions was given by the force field of Snurr et al. [60] For the zeolite atoms, the force field from one of our recent works [61], which have been parameterized with the ability to model silanols, was employed. The self-diffusivity of benzene molecules was calculated from the slope of their mean-square displacements by Einstein's equation [62]. The heat of adsorption of benzene molecules onto ZSM-5 structures was calculated by using single-point energy calculations carried out with general utility lattice program (GULP) [63], as explained in previous studies [64], to better understand the effect of silanol defects on the adsorption of benzene.

In the MD simulations, three different benzene loadings (1 benzene, 3 benzene and 5 benzene per u.c.) were utilized to investigate how the diffusivity and the adsorption energy of benzene in silicalite are influenced by nonbonded benzene…benzene interactions, which become more pronounced at high loadings [65]. Finally, three different temperatures (298 K, 348 K and 398 K) were considered for MD simulations, which allow generation of an Arrhenius plot. From the slope of this plot, it was possible to calculate the activation energy (E^{act}) of diffusion, according to the Arrhenius equation [66].

3 Results and Discussion

3.1 Silanol Condensation Reaction

Both cluster reactant and product structures were optimized at the PM7 quantum semi-empirical level of theory. For the TS of the condensation, herein we propose a concerted reaction mechanism in which a silanol protonates a neighboring silanol while a ≡SiO bond is being formed, as can be seen on Fig. 2. The deprotonated silanol (siloxy), ≡SiO⁻, then forms the ≡Si-O-Si≡ bond (thus repairing the defect) while the formed H_2O molecule remains adsorbed to the zeolite. This reaction shows an "early" TS

in which the proton is transferred between silanols, and the siloxy group formed is just beginning to form a ≡Si-O-Si≡ linkage. This TS has an activation energy of $166\,kJ\,mol^{-1}$ with respect to the initial energy of the reactants. The overall reaction is exergonic by $-46\,kJ\,mol^{-1}$, in agreement to the early TS observed, and hence the reverse hydrolysis reaction has a larger activation barrier, of $166\,kJ\,mol^{-1} + 46\,kJ\,mol^{-1} = 212\,kJ\,mol^{-1}$.

3.2 Heat of Adsorption of Benzene in Silicalite with and without Silanol Defects

The heats of adsorption values are essential in order to check the accuracy of the force field methodology used since its comparison to experimental results is far more reliable than with diffusivity values. A wealth of accurately calculated and experimental values of heat of benzene adsorption in silicalite are available in the literature, and a balanced summary is shown in Fig. 3. The effect of loading is always important, in general, for adsorbates in zeolites. Still, in the case of benzene and silicalite, this is a unique issue due to the rather tight fit of benzene in the medium pore channels to silicalite's inherent flexibility. This is why so many experimental determinations of the silicalite structure are available in the literature, such as those by Olson et al. [36] in 1981, van Koningsveld et al. [67] in 1987 (Pnma), van Koningsveld et al. [68] in 1989 (Pm2m), and van Koningsveld et al. [69] in 1990 (P21/m). Each of these structures leads to slightly different pore sizes which have been analyzed, together with the accuracy with which they can be calculated using four force fields in a recent study in our group [54]. In particular, silicalite undergoes a phase
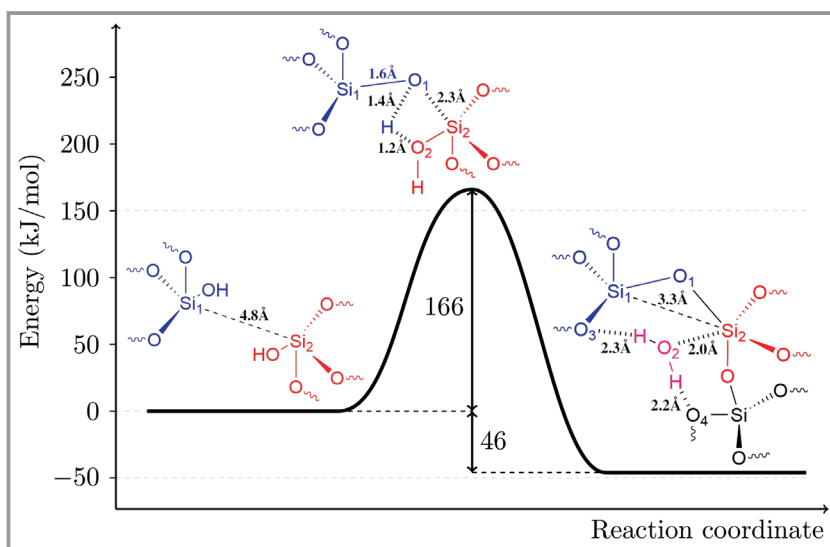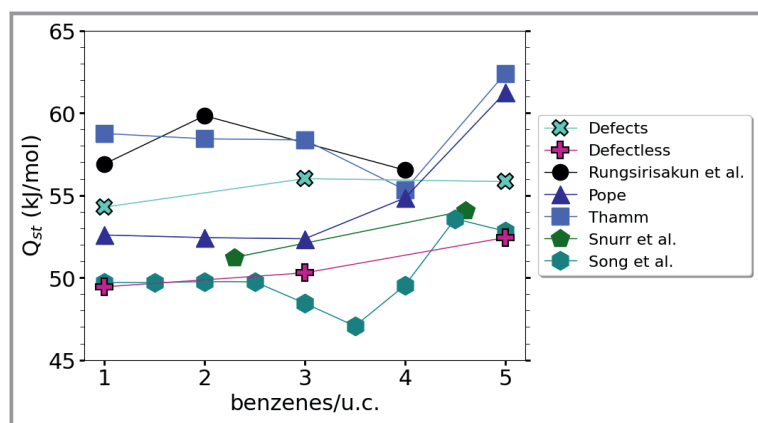

Figure 2. Scheme of the silanol condensation reaction (2≡SiOH → ≡SiOSi≡ + H_2O), showing the relevant distances of reactants, TS, and products with an adsorbed H_2O molecule, within the potential energy diagram through the reaction coordinate, in $kJ\,mol^{-1}$. The full cluster employed in the quantum chemistry semiempirical PM7 calculations is shown in Fig. S3.

transition upon benzene uptake with the so-called ortho (below 6 molecules per u.c.) and para (between 6–8 molecules per u.c.) phases, and also another phase transition triggered by temperature from the orthorhombic Pnma to the triclinic phase P21/m at temperatures below 350 K [70]. Since our calculation of heat of adsorption has been performed below 6 molecules per u.c. (1, 3, and 5), the particularities of phase transition do not need to be taken into account. In principle, this effect should not be a problem to be tackled by the force field when using, as it is the case, fully flexible molecular dynamics, since all calculations are made in P1 cells, which do not imply any symmetry constraints that may limit the structural features associated to a phase transition.

Our results in Fig. 3 indicate, for the defectless silicalite, a close agreement to the experimental results by Song et al. [71] (within 1.8 kJ mol^{-1}), Pope [72] (within 3.1 kJ mol^{-1}, except at the higher benzene loading), and calculated by Snurr et al. [73], while they show less agreement (within 5–10 kJ mol^{-1}) with the results by Thamm [74] or the computational results by Rungirisakun et al. [75]. The latter study adjusted the Lennard-Jones parameters for zeolite···benzene interactions in order reproduce the experimental heat of adsorption of –57.6 kJ mol^{-1} reported by Jänchen and co-workers [76], presenting a good agreement with our results considering defects. Importantly, our zeolite···guest Lennard-Jones parameters were taken from the study of Snurr et al. [60] and this is of course the main reason for the agreement, although in this study a flexible silicalite has been taken into account. Besides, our calculated values are obtained from an average of 10 molecular dynamics configurations at the corresponding loading which have been geometry-optimized.

A neat effect of increase, of 3.4–5.7 kJ mol^{-1}, in our calculated heat of adsorption is observed when changing from the defectless ZSM-5 to the structure with defects. This is due to the specific interactions of the silanol groups with

the benzene molecule as well as the structural silicalite deformation induced by the silanol defects. Since the defects introduced correspond to a very accurate experimental characterization, we believe the structure with defects represents a more realistic model of the silicalite and the corresponding heats of adsorption should be considered for comparison to experiments, in which our Q_{st} varied (in magnitude) from 1.6 to 7.5 kJ mol^{-1}. Further details are available in the SI (Sect. S5).

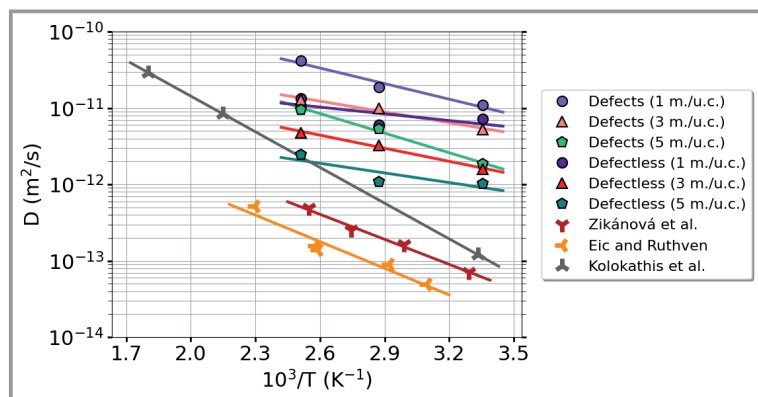### 3.3 Self-Diffusivity of Benzene in Silicalite with and without Silanol Defects

Self-diffusion coefficients (D) obtained (Fig. 4) allow to assess the effects of loading, temperature and structural defects, and are also compared to experimental results in the literature. Regarding the latter, unfortunately our results are between one and two orders of magnitude larger than those obtained from experiments. Although initially, only results from PFG NMR, QENS, and NSE techniques provide measurements of self-diffusivity, a study by Förste et al. [77] for benzene in silicalite demonstrated that corrected diffusivities can also be used in this case, and hence the results by Zikanova et al. [78] obtained with piezoelectric methods, and that by Ruthven et al. [79] obtained with zero length chromatography have been included for comparison.

Since the heats of adsorption are in good agreement with experiments, the reason why self-diffusivities are so large must be found in the values of zeolite···benzene interactions in the less attractive region of the diffusion path. In fact, from the self-diffusivity at different temperatures, an Arrhenius plot (see SI, Sect. S3) allows to calculate the energy barrier for benzene diffusion, and values in the range 6–16 kJ mol^{-1} have been obtained, in stark contrast with experimental values in the range 20–30 kJ mol^{-1} [78, 79, 81–84].

It is therefore expected that if the repulsive part of the zeolite···benzene interactions is improved, a better behavior for diffusion could be easily obtained.
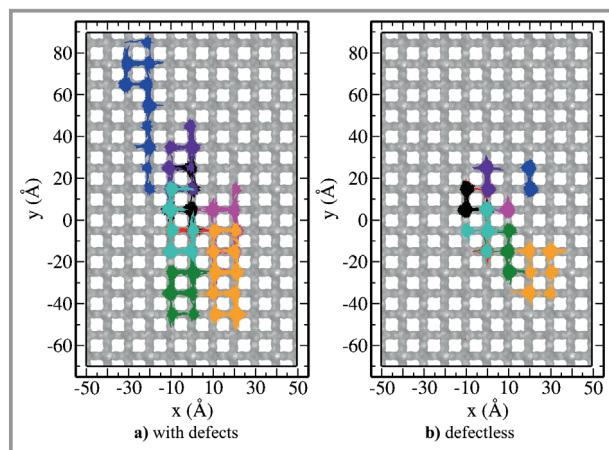
Regarding the loading, the expected effect of decreasing diffusivity with increasing loading (1, 3, 5 benzene per u.c.) is obtained due to the stronger mutual hindrance between benzene molecules and the increasing number of short-distance benzene···benzene events at higher loadings. The studies by Förste et al. [77] and Cartarius et al. [85] include self-diffusivity data for different benzene loadings in silicalite, confirming this trend.

Finally, the most important effect investigated in this manuscript, the main aim, is the effect of silicalite defects on the diffusivity of benzene. The results (Fig. 4) show a difference slightly smaller than an order of magnitude, but with a clear and consistent trend that self-diffusivity

Figure 3. Calculated and experimental heat of adsorption (Q_{st}) of benzene in pure silica MFI (silicalite) at different loadings. Simulated results in this work refer to the framework with and without defects (defects and defectless, respectively). Comparison with data from Rungsirisakun et al. (simulated at 300 K) [75], Pope (323 K) [72], Thamm (301 K) [74], Song et al. [71], and Snurr et al. (334 K) [73]. Lines only for eye guide.

Figure 4. Arrhenius plot for diffusion of benzene in silicalite. Simulated self-diffusion coefficients for framework with defects and defectless, with different benzene loadings (molecules per u.c.). Experimental data from Zikánová et al. [78], Eic and Ruthven (low benzene concentration, within the Henry's Law region) [79], and simulated data from Kolokathis et al. [80] (3 benzenes per u.c.).

increases when defects are taken into account. This is also visually appreciated from the comparison of benzene diffusion trajectories in silicalite with (Fig. 5a) and without defects (Fig. 5b), with the former showing larger mobility. More details of the trajectories can be found in Sect. S4 of the SI. This may seem somewhat surprising at first glance since, as seen above, the structure with defects leads to a larger heat of adsorption and stronger adsorption is usually associated with slower diffusivity. However, as also discussed above, the adsorption paths are only a part of the different locations sampled by a molecule along the diffusion path through the zeolite micropores. Hence, in order to check whether some other structural differences may explain the larger diffusivity observed when defects are present, we analyzed the micropore volumes of both silica-

lites, with and without defects, using Zeo++ software [86]. Tab. S5 (SI) indicates a consistent trend of slightly wider values for the 'largest sphere that can diffuse' parameter in the case of silicalite with defects (additional analysis can be found in Sect. S6, SI). This can be also justified by the fact that intracrystalline silanol defects do not protrude into the channels and, instead, they tend to occupy space outside, although very close, the micropore volume, hence leaving more room for diffusing molecules. This is the opposite to the case of some Brønsted acid sites which, by protruding inside the channels, contribute to decrease self-diffusivity [87]. Since, as said above, benzene is a molecule fitting tightly into the medium pore channels of silicalite, this small extra-space in the silicalite with defects could be enough to explain the larger diffusivity.

It could be argued against this explanation by stating that perhaps the zeolite force field employed is enlarging the micropore size above its experimental value, particularly in the case of the zeolite with defects. In order to test this hypothesis, molecular dynamics simulations have also been done with a rigid framework, in which the experimental structure of silicalite is employed. For the structure with defects, only the atomic coordinates of the intracrystalline silanols have been initially geometry-optimized and then all the atoms of the defective unit cell have been kept rigid for the molecular dynamics runs. The results obtained (Sect. S3, SI) indicate a minor effect of smaller diffusion coefficients with respect to the fully flexible framework case. This affects both the silicalite with and without defects and is observed equally for all loadings and all temperatures. Hence, the above conclusion that the intracrystalline silanol defects contribute to increase the self-diffusivity is confirmed. Our interpretation, as stated above, is that silicalite defects tend to protrude outside the micropore space, providing slightly more room for the diffusion of benzene molecules.

Some previous experimental studies seem to support these results. Vidoni et al. [88] explored the adsorption of CO_2 on pure silica MFI and DDR zeolites containing various amounts of structural defects by combining experimental and computational methods. They concluded that an increased CO_2 adsorption capacity is achieved in defective MFI and DDR structures due to a larger pore volume and partial access to the small cages, respectively, caused by defects. While studying the internal silanol groups in silicalite, Hunger et al. [89] found that the molecular mobility of the sorbed benzene molecules increases as the defect content of the zeolite increases, possibly due to the further sorbate-induced deformation in the structure with more defects, in agreement with our findings.

Furthermore, the enhanced diffusion of benzene, at all temperatures and adsorbate loadings, when the defects are present is in agreement with the experimental data from

Figure 5. Benzene trajectories from molecular dynamics simulations at 348 K, over 100 ns and considering a flexible silicalite framework. MFI channel system depicted in gray, and each benzene molecule with a different color (8 molecules in a 2×2×2 silicalite cell, 1 molecule per u.c.). Silicalite framework a) with defects and b) without defects.

Song et al. [71] (Tab. S2, SI). Although we can reproduce this trend, our simulated self-diffusion coefficient is approximately two orders of magnitude higher than the experimental data of Song and co-workers (Fig. S10, SI). Moreover, among our simulated results considering defects, benzene diffusion is enhanced in 1.5–2.6 times when framework flexibility is taken into account (solid and dashed lines in Fig. S10a, SI). The E^{act} was calculated for our simulated data and Song et al. experimental samples with and without internal defects (Tab. S3, SI). For the experimental samples, the slower diffusion is associated with higher E^{act} values. Therefore, sample B (defectless) presented activation energies in a range 29–37 kJ mol^{-1}, that decreases to 23–29 kJ mol^{-1} when the internal silanols are present. Our simulated data overestimates the diffusion of benzene, and consequently, smaller E^{act} values should be expected. Indeed, our simulated data predicts a diffusion barrier of 9–16 kJ mol^{-1} if defects are present.

4   Conclusions

A large effort in the last decades has been done for the accurate measurement and interpretation of self-diffusivity of molecules in zeolites, and in particular silicalite has been one of the most studied. Computer simulations have also, in parallel, tried to provide an atomistic view of this phenomenon. A challenging case is benzene and other aromatic molecules since they fit tightly in the 10-ring channels of silicalite and then not only the attractive but also the repulsive part of the zeolite···benzene interactions need to be calculated accurately. After several decades of intensive attempts, there are still not straightforward molecular dynamics studies reproducing the order of magnitude of the self-diffusivity at different loadings and temperatures. This is in part due to the small self-diffusivity that requires too long simulation times in order to obtain statistically meaningful results. Although our present study does not achieve this accuracy, our goal was to study the effects of silicalite defects on self-diffusivity. Since there is experimental work, mainly based on cross polarization ^{1}H ^{29}Si MAS NMR, giving an accurate characterization of intracrystalline silanol groups of silicalite, we have made realistic computational models that allow comparison of the resulting self-diffusivity of benzene with the usually employed model of a defectless silicalite. The results show heats of adsorption in good agreement (within 5 kJ mol^{-1}, on average) with experiments over the studied loading (1, 3, 5 benzene per u.c.), with always larger heat of adsorption for the silicalite with defects compared to the defectless structure. Regarding the activation barriers, values in the range of 6–16 kJ mol^{-1} have been obtained, notably smaller than the experimentally measured (ca. 20–30 kJ mol^{-1}). The comparison of self-diffusivity of benzene in silicalite with and without defects indicates a clear trend of larger diffusivity (ca. 2–5 times) for the silicalite with defects that we assess to a slightly

larger micropore space available due to the fact that defects tend to protrude outside the micropore, as demonstrated by the specific characterization of the largest sphere that can diffuse in both cases.

This effect could be more pronounced in samples with larger amounts of defects than those considered here (4 % of the T sites) for the silicalite synthesized using tetrapropylammonium as structure directing agent. The currently advanced characterization of zeolite defects, as well as the availability of increasingly more robust force fields, allows to make accurate models of pure silica zeolites with defects that should be replacing the traditionally used pure silica without defects. Although of course silica zeolites without a significant amount of defects are also employed in a considerable number of processes, defects also arise in these cases after prolonged use and their effect on performance can be studied and compared with ideal crystals in order to elucidate how they contribute to the observed results.

Supporting Information

Supporting Information for this article can be found under DOI: https://doi.org/10.1002/cite.202300008. It contains further information regarding the model of silicalite with defects, mean square displacements, self-diffusion coefficients, benzene trajectories from molecular dynamics, adsorption energies, and micropore analysis. Also included is a CIF file of the defective silicalite, and XZY files with the cluster geometries corresponding to the silanol condensation reaction.

Symbols Used

D	[m^{2}s^{-1}]	self-diffusion coefficient
E^{act}	[kJ mol^{-1}]	activation energy
Q_{st}	[kJ mol^{-1}]	heat of adsorption

Abbreviations

GULP	general utility lattice program
MAS	magic angle spinning

MC	Monte Carlo
MD	molecular dynamics
MTO	methanol-to-olefin
NMR	nuclear magnetic resonance
NSE	neutron spin echo
OPLS	optimized potentials for liquid simulations
OSDA	organic structure-directing agent
PFG	pulse field gradient
QENS	quasi-elastic neutron scattering
TS	transition state
u.c.	unit cell

References

[1] Y. Li, J. Yu, *Chem. Rev.* **2014**, *114 (14)*, 7268–7316. DOI: https://doi.org/10.1021/cr500010r

[2] E. Pérez-Botella, S. Valencia, F. Rey, *Chem. Rev.* **2022**. DOI: https://doi.org/10.1021/acs.chemrev.2c00140

[3] M. Kumar et al., *J. Am. Chem. Soc.* **2019**, *141 (51)*, 20155–20165. DOI: https://doi.org/10.1021/jacs.9b09697

[4] C. Baerlocher, D. Xie, L. B. McCusker, S.-J. Hwang, I. Y. Chan, K. Ong, A. W. Burton, S. I. Zones, *Nat. Mater.* **2008**, *7 (8)*, 631–635. DOI: https://doi.org/10.1038/nmat2228

[5] M. A. Camblor, C. Corell, A. Corma, M.-J. Díaz-Cabañas, S. Nicolopoulos, J. M. González-Calbet, M. Vallet-Regí, *Chem. Mater.* **1996**, *8 (10)*, 2415–2417. DOI: https://doi.org/10.1021/cm960322v

[6] M. A. Camblor, A. Corma, M.-J. Díaz-Cabañas, C. Baerlocher, *J. Phys. Chem. B* **1998**, *102 (1)*, 44–51. DOI: https://doi.org/10.1021/jp972319k

[7] J. M. Chezeau, L. Delmotte, J. L. Guth, Z. Gabelica, *Zeolites* **1991**, *11 (6)*, 598–606. DOI: https://doi.org/10.1016/S0144-2449(05)80011-9

[8] E. E. Mallon, M. Y. Jeon, M. Navarro, A. Bhan, M. Tsapatsis, *Langmuir* **2013**, *29 (22)*, 6546–6555. DOI: https://doi.org/10.1021/la4001494

[9] J. E. Schmidt, D. Xie, M. E. Davis, *J. Mater. Chem. A* **2015**, *3 (24)*, 12890–12897. DOI: https://doi.org/10.1039/C5TA02354H

[10] L. Schreyeck, P. Caullet, J. C. Mougenel, J. L. Guth, B. Marler, *Microporous Mater.* **1996**, *6 (5)*, 259–271. DOI: https://doi.org/10.1016/0927-6513(96)00032-6

[11] T. Moteki, W. Chaikittisilp, A. Shimojima, T. Okubo, *J. Am. Chem. Soc.* **2008**, *130 (47)*, 15780–15781. DOI: https://doi.org/10.1021/ja806930h

[12] T. Kawai, K. Tsutsumi, *J. Colloid Interface Sci.* **1999**, *212 (2)*, 310–316. DOI: https://doi.org/10.1006/jcis.1999.6093

[13] A. Palčić, S. Moldovan, H. El Siblani, A. Vicente, V. Valtchev, *Adv. Sci.* **2022**, *9 (4)*, 2104414. DOI: https://doi.org/10.1002/advs.202104414

[14] H. Koller, R. F. Lobo, S. L. Burkett, M. E. Davis, *J. Phys. Chem.* **1995**, *99 (33)*, 12588–12596. DOI: https://doi.org/10.1021/j100033a036

[15] G. Brunklaus, H. Koller, S. I. Zones, *Angew. Chem., Int. Ed.* **2016**, *55 (46)*, 14459–14463. DOI: https://doi.org/10.1002/anie.201607428

[16] P. Eliášová, M. Opanasenko, P. S. Wheatley, M. Shamzhy, M. Mazur, P. Nachtigall, W. J. Roth, R. E. Morris, J. Čejka, *Chem. Soc. Rev.* **2015**, *44 (20)*, 7177–7206. DOI: https://doi.org/10.1039/C5CS00045A

[17] I. C. Medeiros-Costa, E. Dib, N. Nesterenko, J.-P. Dath, J.-P. Gilson, S. Mintova, *Chem. Soc. Rev.* **2021**, *50 (19)*, 11156–11179. DOI: https://doi.org/10.1039/D1CS00395J

[18] E. Janiszewska, A. Macario, J. Wilk, A. Aloise, S. Kowalak, J. B. Nagy, G. Giordano, *Microporous Mesoporous Mater.* **2013**, *182*, 220–228. DOI: https://doi.org/10.1016/j.micromeso.2012.12.013

[19] I. Yarulina, J. Goetze, C. Gücüyener, L. van Thiel, A. Dikhtiarenko, J. Ruiz-Martinez, B. M. Weckhuysen, J. Gascon, F. Kapteijn, *Catal. Sci. Technol.* **2016**, *6 (8)*, 2663–2678. DOI: https://doi.org/10.1039/C5CY02140E

[20] Z. Qin, L. Lakiss, L. Tosheva, J.-P. Gilson, A. Vicente, C. Fernandez, V. Valtchev, *Adv. Funct. Mater.* **2014**, *24 (2)*, 257–264. DOI: https://doi.org/10.1002/adfm.201301541

[21] A. Li, Y. Zhang, C. J. Heard, K. Gołąbek, X. Ju, J. Čejka, M. Mazur, *Angew. Chem., Int. Ed.* **2023**, *62 (1)*, e202213361. DOI: https://doi.org/10.1002/anie.202213361

[22] F. Dubray, S. Moldovan, C. Kouvatas, J. Grand, C. Aquino, N. Barrier, J.-P. Gilson, N. Nesterenko, D. Minoux, S. Mintova, *J. Am. Chem. Soc.* **2019**, *141 (22)*, 8689–8693. DOI: https://doi.org/10.1021/jacs.9b02589

[23] S. V. Konnov et al., *Angew. Chem., Int. Ed.* **2020**, *59 (44)*, 19553–19560. DOI: https://doi.org/10.1002/anie.202006524

[24] H. Y. Luo, L. Bui, W. R. Gunther, E. Min, Y. Román-Leshkov, *ACS Catal.* **2012**, *2 (12)*, 2695–2699. DOI: https://doi.org/10.1021/cs300543z

[25] Y. Ye, M. Yao, H. Chen, X. Zhang, *Catal Lett.* **2020**, *150 (5)*, 1445–1453. DOI: https://doi.org/10.1007/s10562-019-03040-x

[26] W. Zhou, J. Liu, J. Wang, L. Lin, N. He, X. Zhang, H. Guo, *Catalysts* **2019**, *9 (7)*, 571. DOI: https://doi.org/10.3390/catal9070571

[27] H. Jobic, W. Schmidt, C. B. Krause, J. Kärger, *Microporous Mesoporous Mater.* **2006**, *90 (1)*, 299–306. DOI: https://doi.org/10.1016/j.micromeso.2005.10.020

[28] J. Kärger, M. Bülow, P. Lorenz, *J. Colloid Interface Sci.* **1978**, *65 (1)*, 181–185. DOI: https://doi.org/10.1016/0021-9797(78)90270-9

[29] A. Germanus, J. Kärger, H. Pfeifer, N. N. Samulevič, S. P. Zdanov, *Zeolites* **1985**, *5 (2)*, 91–95. DOI: https://doi.org/10.1016/0144-2449(85)90079-X

[30] J. Kärger, M. Avramovska, D. Freude, J. Haase, S. Hwang, R. Valiullin, *Adsorption.* **2021**, *27 (3)*, 453–484. DOI: https://doi.org/10.1007/s10450-020-00290-9

[31] S. Caro-Ortiz, E. Zuidema, M. Rigutto, D. Dubbeldam, T. J. H. Vlugt, *J. Phys. Chem. C.* **2020**, *124 (44)*, 24488–24499. DOI: https://doi.org/10.1021/acs.jpcc.0c08054

[32] E. J. Maginn, A. T. Bell, D. N. Theodorou, *J. Phys. Chem.* **1993**, *97 (16)*, 4173–4181. DOI: https://doi.org/10.1021/j100118a038

[33] A. I. Skoulidas, D. S. Sholl, *J. Phys. Chem. B.* **2002**, *106 (19)*, 5058–5067. DOI: https://doi.org/10.1021/jp014279x

[34] T. F. Degnan, G. K. Chitnis, P. H. Schipper, *Microporous Mesoporous Mater.* **2000**, *35–36*, 245–252. DOI: https://doi.org/10.1016/S1387-1811(99)00225-5

[35] B. Hunger, S. Matysik, M. Heuchel, W.-D. Einicke, *Langmuir* **1997**, *13 (23)*, 6249–6254. DOI: https://doi.org/10.1021/la970615i

[36] D. H. Olson, G. T. Kokotailo, S. L. Lawton, W. M. Meier, *J. Phys. Chem.* **1981**, *85 (15)*, 2238–2243. DOI: https://doi.org/10.1021/j150615a020

[37] J. Kärger, D. M. Ruthven, in *Diffusion in Zeolites and Other Microporous Solids*, 1st ed., John Wiley, New York **1992**.

[38] S. Vasenkov, W. Böhlmann, P. Galvosas, O. Geier, H. Liu, J. Kärger, *J. Phys. Chem. B.* **2001**, *105 (25)*, 5922–5927. DOI: https://doi.org/10.1021/jp003899f

[39] J. Kärger, H. Pfeifer, E. Riedel, H. Winkler, *J. Colloid Interface Sci.* **1973**, *44 (1)*, 187–188. DOI: https://doi.org/10.1016/0021-9797(73)90208-7

[40] J. Kärger, J. Caro, *J. Chem. Soc., Faraday Trans. 1* **1977**, *73*, 1363–1376. DOI: https://doi.org/10.1039/F19777301363

[41] H. Jobic, A. Méthivier, *Oil Gas Sci. Technol.* **2005**, *60 (5)*, 815–830. DOI: https://doi.org/10.2516/ogst:2005058

[42] H. Paoli, A. Méthivier, H. Jobic, C. Krause, H. Pfeifer, F. Stallmach, J. Kärger, *Microporous Mesoporous Mater.* **2002**, *55 (2)*, 147–158. DOI: https://doi.org/10.1016/S1387-1811(02)00399-2

[43] M. J. Frisch et al., *Gaussian 16*, Revision A.03, Gaussian, Inc., Wallingford, CT **2016**.

[44] J. J. P. Stewart, *J. Mol. Model.* **2013**, *19 (1)*, 1–32. DOI: https://doi.org/10.1007/s00894-012-1667-x

[45] P. Jurečka, J. Černý, P. Hobza, D. R. Salahub, *J. Comput. Chem.* **2007**, *28 (2)*, 555–569. DOI: https://doi.org/10.1002/jcc.20570

[46] J. Řezáč, J. Fanfrlík, D. Salahub, P. Hobza, *J. Chem. Theory Comput.* **2009**, *5 (7)*, 1749–1760. DOI: https://doi.org/10.1021/ct9000922

[47] M. Korth, M. Pitoňák, J. Řezáč, P. Hobza, *J. Chem. Theory Comput.* **2010**, *6 (1)*, 344–352. DOI: https://doi.org/10.1021/ct900541n

[48] J. Řezáč, P. Hobza, *J. Chem. Theory Comput.* **2012**, *8 (1)*, 141–151. DOI: https://doi.org/10.1021/ct200751e

[49] P. Jurečka, J. Šponer, J. Černý, P. Hobza, *Phys. Chem. Chem. Phys.* **2006**, *8 (17)*, 1985–1993. DOI: https://doi.org/10.1039/B600027D

[50] K. Fukui, *Acc. Chem. Res.* **1981**, *14 (12)*, 363–368. DOI: https://doi.org/10.1021/ar00072a001

[51] W. Smith, T. R. Forester, *J. Mol. Graphics* **1996**, *14 (3)*, 136–141. DOI: https://doi.org/10.1016/S0263-7855(96)00043-4

[52] L. Verlet, *Phys. Rev.* **1967**, *159 (1)*, 98–103. DOI: https://doi.org/10.1103/PhysRev.159.98

[53] W. G. Hoover, *Phys. Rev. A.* **1985**, *31 (3)*, 1695–1697. DOI: https://doi.org/10.1103/PhysRevA.31.1695

[54] D. Bermúdez, G. Sastre, *Theor. Chem. Acc.* **2017**, *136 (10)*, 116. DOI: https://doi.org/10.1007/s00214-017-2143-6

[55] H. Goldstein, C. Poole, J. Safko, *Am. J. Phys.* **2002**, *70 (7)*, 782–783. DOI: https://doi.org/10.1119/1.1484149

[56] P. P. Ewald, *Ann. Phys.* **1921**, *369 (3)*, 253–287. DOI: https://doi.org/10.1002/andp.19213690304

[57] L. S. Tee, S. Gotoh, W. E. Stewart, *Ind. Eng. Chem. Fund.* **1966**, *5 (3)*, 356–363. DOI: https://doi.org/10.1021/i160019a011

[58] T. Oie, G. M. Maggiora, R. E. Christoffersen, D. J. Duchamp, *Int. J. Quantum Chem.* **1981**, *20 (S8)*, 1–47. DOI: https://doi.org/10.1002/qua.560200703

[59] W. L. Jorgensen, D. S. Maxwell, J. Tirado-Rives, *J. Am. Chem. Soc.* **1996**, *118 (45)*, 11225–11236. DOI: https://doi.org/10.1021/ja9621760

[60] R. Q. Snurr, A. T. Bell, D. N. Theodorou, *J. Phys. Chem.* **1994**, *98 (46)*, 11948–11961. DOI: https://doi.org/10.1021/j100097a022

[61] A. Misturini, F. Rey, G. Sastre, *J. Phys. Chem. C* **2022**, *126 (41)*, 17680–17691. DOI: https://doi.org/10.1021/acs.jpcc.2c04331

[62] A. Einstein, *Investigations on the Theory of the Brownian Movement*, Courier Corporation **1956**.

[63] J. D. Gale, *J. Chem. Soc., Faraday Trans.* **1997**, *93 (4)*, 629–637. DOI: https://doi.org/10.1039/A606455H

[64] E. Pérez-Botella, A. Misturini, A. Sala, M. Palomino, A. Corma, G. Sastre, S. Valencia, F. Rey, *J. Phys. Chem. C* **2020**, *124 (49)*, 26821–26829. DOI: https://doi.org/10.1021/acs.jpcc.0c08517

[65] H. Zheng, L. Zhao, Q. Yang, S. Dang, Y. Wang, J. Gao, C. Xu, *RSC Adv.* **2016**, *6 (41)*, 34175–34187. DOI: https://doi.org/10.1039/C6RA02338J

[66] S. Arrhenius, *Z. Phys. Chem.* **1889**, *4U (1)*, 226–248. DOI: https://doi.org/10.1515/zpch-1889-0416

[67] H. Van Koningsveld, H. Van Bekkum, J. C. Jansen, *Acta. Cryst. B* **1987**, *43 (2)*, 127–132. DOI: https://doi.org/10.1107/S0108768187098173

[68] H. van Koningsveld, F. Tuinstra, H. van Bekkum, J. C. Jansen, *Acta. Cryst. B* **1989**, *45 (4)*, 423–431. DOI: https://doi.org/10.1107/S0108768189004519

[69] H. van Koningsveld, J. C. Jansen, H. van Bekkum, *Zeolites* **1990**, *10 (4)*, 235–242. DOI: https://doi.org/10.1016/0144-2449(94)90134-1

[70] H. Van Koningsveld, *Acta. Cryst. B* **1990**, *46 (6)*, 731–735. DOI: https://doi.org/10.1107/S0108768190007522

[71] L. Song, Z.-L. Sun, H.-Y. Ban, M. Dai, L. V. C. Rees, *Phys. Chem. Chem. Phys.* **2004**, *6 (19)*, 4722–4731. DOI: https://doi.org/10.1039/B406051B

[72] C. G. Pope, *J. Phys. Chem.* **1986**, *90 (5)*, 835–837. DOI: https://doi.org/10.1021/j100277a025

[73] R. Q. Snurr, A. T. Bell, D. N. Theodorou, *J. Phys. Chem.* **1993**, *97 (51)*, 13742–13752. DOI: https://doi.org/10.1021/j100153a051

[74] H. Thamm, *J. Phys. Chem.* **1987**, *91 (1)*, 8–11. DOI: https://doi.org/10.1021/j100285a004

[75] R. Rungsirisakun, T. Nanok, M. Probst, J. Limtrakul, *J. Mol. Graphics Modell.* **2006**, *24 (5)*, 373–382. DOI: https://doi.org/10.1016/j.jmgm.2005.10.003

[76] J. Jänchen, H. Stach, L. Uytterhoeven, W. J. Mortier, *J. Phys. Chem.* **1996**, *100 (30)*, 12489–12493. DOI: https://doi.org/10.1021/jp953791d

[77] C. Förste, J. Kärger, H. Pfeifer, L. Riekert, M. Bülow, A. Zikánová, *J. Chem. Soc., Faraday Trans.* **1990**, *86 (5)*, 881–885. DOI: https://doi.org/10.1039/FT9908600881

[78] A. Zikánová, M. Bülow, H. Schlodder, *Zeolites* **1987**, *7 (2)*, 115–118. DOI: https://doi.org/10.1016/0144-2449(87)90070-4

[79] M. Eic, D. M. Ruthven, *Stud. Surf. Sci. Catal.* **1989**, *49*, 897–905. DOI: https://doi.org/10.1016/S0167-2991(08)61976-X

[80] P. D. Kolokathis, E. Pantatosaki, C.-A. Gatsiou, H. Jobic, G. K. Papadopoulos, D. N. Theodorou, *Mol. Simul.* **2014**, *40 (1–3)*, 80–100. DOI: https://doi.org/10.1080/08927022.2013.840895

[81] D. B. Shah, D. T. Hayhurst, G. Evanina, C. J. Guo, *AIChE Journal.* **1988**, *34 (10)*, 1713–1717. DOI: https://doi.org/10.1002/aic.690341016

[82] N. Van-Den-Begin, L. V. C. Rees, J. Caro, M. Bülow, *Zeolites* **1989**, *9 (4)*, 287–292. DOI: https://doi.org/10.1016/0144-2449(89)90073-0

[83] D. M. Ruthven, M. Eic, E. Richard, *Zeolites* **1991**, *11 (7)*, 647–653. DOI: https://doi.org/10.1016/S0144-2449(05)80166-6

[84] D. Shen, L. V. C. Rees, *Zeolites* **1991**, *11 (7)*, 666–671. DOI: https://doi.org/10.1016/S0144-2449(05)80169-1

[85] R. Cartarius, H. Vogel, J. Dembowski, *Ber. Bunsen-Ges.* **1997**, *101 (2)*, 193–199. DOI: https://doi.org/10.1002/bbpc.19971010206

[86] T. F. Willems, C. H. Rycroft, M. Kazi, J. C. Meza, M. Haranczyk, *Microporous Mesoporous Mater.* **2012**, *149 (1)*, 134–141. DOI: https://doi.org/10.1016/j.micromeso.2011.08.020

[87] Z. A. Alaithan, N. Harrison, G. Sastre, *J. Phys. Chem. C* **2021**, *125 (35)*, 19200–19208. DOI: https://doi.org/10.1021/acs.jpcc.1c04090

[88] A. Vidoni, P. I. Ravikovitch, M. Afeworki, D. Calabro, H. Deckman, D. Ruthven, *Microporous Mesoporous Mater.* **2020**, *294*, 109818. DOI: https://doi.org/10.1016/j.micromeso.2019.109818

[89] M. Hunger, J. Kärger, H. Pfeifer, J. Caro, B. Zibrowius, M. Bülow, R. Mostowicz, *J. Chem. Soc., Faraday Trans. 1* **1987**, *83 (11)*, 3459–3468. DOI: https://doi.org/10.1039/F19878303459